

Distribution Agreement

In presenting this thesis as a partial fulfillment of the requirements for a degree from Emory University, I hereby grant to Emory University and its agents the non-exclusive license to archive, make accessible, and display my thesis in whole or in part in all forms of media, now or hereafter now, including display on the World Wide Web. I understand that I may select some access restrictions as part of the online submission of this thesis. I retain all ownership rights to the copyright of the thesis. I also retain the right to use in future works (such as articles or books) all or part of this thesis.

Sonia Corbett Karkare

March 24, 2023

Functional mapping of reward responses in the lateral septum along the dorsoventral axis

by

Sonia Corbett Karkare

Dr. Malavika Murugan
Adviser

Neuroscience & Behavioral Biology

Dr. Malavika Murugan
Adviser

Dr. Shannon Gourley
Committee Member

Dr. Larry Young
Committee Member

2023

Functional mapping of reward responses in the lateral septum along the dorsoventral axis

By

Sonia Corbett Karkare

Dr. Malavika Murugan

Adviser

An abstract of
a thesis submitted to the Faculty of Emory College of Arts and Sciences
of Emory University in partial fulfillment
of the requirements of the degree of
Bachelor of Science with Honors

Neuroscience & Behavioral Biology

2023

Abstract

Functional mapping of reward responses in the lateral septum along the dorsoventral axis

By Sonia Corbett Karkare

The lateral septum (LS) has been implicated in a wide range of behaviors, including aggression, reward-related behaviors, kin recognition, sexual behaviors, and social memory. While the specific role of the LS in mediating such a variety of behaviors is unclear, its anatomical heterogeneity has been suggested as a putative contributor to its functional diversity. Discrete LS compartments have been identified by specific properties, such as connectivity with the hippocampus and hypothalamus, as well as the differential expression of receptors and neuropeptides. Recent evidence suggests that subregions of the LS might play a role in modulating both approach and avoidance behaviors. In particular, there appears to be functional clustering of neurons along the dorsoventral (DV) axis within the LS, with approach behaviors modulated by neurons localized to the dorsal subdivision of the LS, while avoidance behaviors are mediated by neurons in the ventral LS. However, it is unclear how reward responses are organized along the DV axis of the LS. In this study, we performed monosynaptic rabies tracing experiments to characterize the patterns of inputs to different LS projection populations. Additionally, we performed cellular resolution calcium imaging in different positions along the DV axis of the LS during an operant reward task to determine how reward responses are organized along the DV axis of the LS. We did not find significant differences in proportions of input neurons to the projection populations in our tracing experiments suggesting that different LS projection populations receive similar patterns of inputs across various brain regions. We found interesting differences in the reward-related activity along the DV axis in the pilot cohort of animals suggesting that dorsal and ventral populations of LS likely play different roles in reward-related behaviors. Future studies will be required to validate this result, as well as to further ascertain the identities of the imaged neurons and the causal role they play in mediating behavior.

Functional mapping of reward responses in the lateral septum along the dorsoventral axis

By

Sonia Corbett Karkare

Dr. Malavika Murugan

Adviser

A thesis submitted to the Faculty of Emory College of Arts and Sciences
of Emory University in partial fulfillment
of the requirements of the degree of
Bachelor of Science with Honors

Neuroscience & Behavioral Biology

2023

Acknowledgements

I would like to thank Dr. Malavika Murugan for giving me the opportunity to join her lab and be a part of many exciting projects. My time in the lab has defined my undergraduate experience, and this would not have been possible without her.

I would like to thank Jenni Isaac for her mentorship and support over the past two years. Everything I have learned and accomplished in the lab can be traced back to her. I also appreciate her willingness to read my writing, even though she hates my run-on sentences.

I would like to thank my fellow lab members for their support and encouragement as well: Sarah Thomas, for being my lab partner in crime; Maha Rashid, for her incredible wrist strength to untighten anything in lab; Hyma Balasubramanian, for her willingness to train another undergraduate to help me with analysis; and Chris Feng, for being able to pull interesting results from a massive dataset.

Finally, I would like to thank my family for being willing to sit through my practice presentations of this data, despite their lack of interest in the lateral septum.

Table of Contents

Introduction.....	1
Anatomy of the LS.....	2
Figure 1: Divisions of the LS.....	2
LS connectivity.....	3
mRNA distribution.....	3
DV organization of the LS.....	5
Approach, avoidance, and aggression.....	5
Reward.....	6
Aims and results.....	7
Results.....	8
LS projection populations receive largely overlapping brain-wide inputs.....	8
Figure 2: Monosynaptic rabies tracing.....	9
Figure 3: Wholebrain software analysis.....	9
Figure 4: Anatomical locations of subcortical downstream targets of the LS.....	10
Figure 5: Distributions of monosynaptic inputs to LS projection populations.....	12
Figure 6: Quantification of monosynaptic inputs to LS projection populations.....	13
Starter cell populations occupy distinct compartments of the LS.....	14
Figure 7: Representative starter cell locations along the DV axis of the LS.....	14
Both excitatory and inhibitory reward-responsive neurons are found along the LS DV axis....	15
Figure 8: Cellular resolution calcium imaging.....	15
Figure 9: Behavioral paradigm and example results.....	17
Figure 10: Time-locked excitatory and inhibitory reward-responses of LS neurons	

along the DV axis.....	18
Excitatory reward-responsive neurons show varying temporal dynamics in the dorsal and ventral LS.....	19
Figure 11: Temporal dynamics of excitatory reward responses in LSd, LSi, and LSv...	20
Activity of LS neurons differs on rewarded and unrewarded trials.....	22
Figure 12: Decoding of neural activity on rewarded and unrewarded trials.....	22
Discussion.....	24
Anatomically positioned as a functional hub rather than relay station.....	24
Temporal dynamics of LS reward responses along the DV axis.....	25
Lateral inhibition.....	26
Limitations and future directions.....	27
Figure 12: Tracking neurons across training.....	28
Methods.....	29
References.....	36

Introduction

The lateral septum (LS) is a largely GABAergic brain region situated medial to the lateral ventricles and ventral to the corpus callosum (Rizzi-Wise & Wang, 2021). Initial studies of the LS identified a role for the region in mediating reward behaviors and aggression. Specifically, lesioning the LS resulted in a hyperaggressive phenotype termed “septal rage” in multiple rodent species (Albert & Chew, 1980; Potegal et al., 1981; Schnurr, 1972; Slotnick et al., 1973). However, researchers also observed changes in feeding behavior, sexual behavior, and reward-related behavior with LS lesions (Albert & Chew, 1980; Kishore & Desiraju, 1990; Potegal et al., 1981). Intriguingly, studies found that septal lesions abolished the reinforcing effects of intracranial stimulation of the ventral tegmental area (VTA), an area well known for its vital role in reward consumption and addiction (Cai & Tong, 2022; Kishore & Desiraju, 1990). These initial studies paved the way for a series of experiments that systematically mapped the behavioral effects of lesioning smaller subregions of the LS. For example, it was established that lesions of the ventral, but not dorsal portion of the LS consistently induced septal rage (Potegal et al., 1981). More recently, studies have identified that neurons in the LSv project strongly to the ventromedial hypothalamic nucleus (vmH), a region heavily implicated in aggression (Guo et al., 2023; Leroy et al., 2018; Nelson & Trainor, 2007; Wong et al., 2016). Moreover, optogenetically and chemogenetically manipulating LSv activity has demonstrated the causal role for these neurons in regulating aggressive behaviors (Wong et al., 2016).

However, the ventral LS only occupies a quarter of the entire LS (Risold & Swanson, 1997a). Furthermore, the LS has been implicated in a wide range of behaviors beyond aggression, including kin recognition, reward behaviors, sexual behaviors, and spatial memory (Clemens et al., 2020; Kishore & Desiraju, 1990; Kondo et al., 1990; Leutgeb & Mizumori, 1999). Recent

studies have speculated that the LS serves as a hub that consolidates cognitive, emotional, and spatial information, primarily from the hippocampus, to modulate behavioral outputs via downstream subcortical targets (Rizzi-Wise & Wang, 2021). Yet, it is unclear how the LS modulates such a wide variety of behaviors. One hypothesis is that distinct anatomical compartments of the LS, likely mapping on to specific projection or cellular populations within the LS, might contribute to the functional heterogeneity attributed to the LS.

Anatomy of the LS

Anatomical studies have established three main compartments of the LS: dorsocaudal (LSd), intermediate-rostral (LSi), and ventral (LSv). These three compartments can be divided into further distinct subregions as defined by either their molecular composition or anatomical connectivity (Risold & Swanson, 1997a).

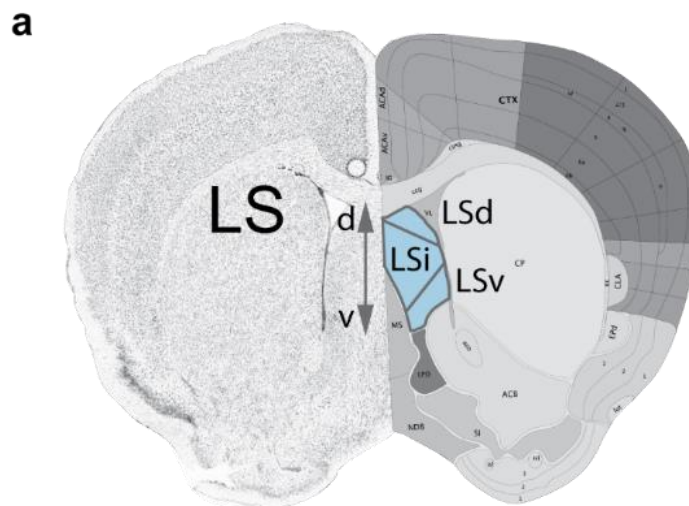


Figure 1. Divisions of the LS. (a) The LS is anatomically divided into 3 compartments defined by their molecular makeup and connectivity.

LS connectivity

All LS compartments receive glutamatergic inputs from the hippocampus, but there are differences in which subregions of the hippocampal formation project to the various LS subregions (Risold & Swanson, 1997a). The LSi and LSv primarily receive projections from CA1 and subiculum (SUB); more specifically, ventral CA1 and ventral subiculum projects preferentially onto the LSv (Risold & Swanson, 1997a). The LSd is the sole compartment to share a bidirectional connection with dorsal CA3 (Risold & Swanson, 1996). The LS compartments also vary in the hypothalamic subregions they project onto (Risold & Swanson, 1997b). In particular, the LSd synapses onto the hypothalamic lateral zone and lateral supramammillary nucleus (Swanson & Cowan, 1979). In contrast, the LSi sends dense projections to the rostral hypothalamic medial zone while the LSv projects to the medial preoptic nucleus, the ventral medial hypothalamic nucleus, and the hypothalamic periventricular zone (Risold & Swanson, 1997b).

mRNA distribution

In addition to the differences in connectivity, the neurons in the various LS subregions also show differences in their molecular profile and chemoarchitecture according to Risold and Swanson, 1997a. Notably, neurons in the LSv do not express somatostatin or enkephalin (an opioid-like pentapeptide) mRNA (Simantov et al., 1977); the mRNA for these proteins are enriched in the LSd and LSi respectively. Neurotensin and enkephalin mRNA is distributed along a gradient within the LSi, with both showing denser expression rostrally and less dense expression towards the caudal end of the LSi. Neurotensin's role as a neuropeptide is diverse, including modulating neurotransmitter systems such as dopamine (DA) release (Boules et al., 2013). In situ hybridization also identified mRNA for dynorphin, growth hormone-releasing hormone (GHRH),

and substance P, although cells expressing these mRNA types were found less frequently within the LS compared to mRNA for somatostatin, enkephalin, or neurotensin. The distribution of dynorphin, another opioid peptide within the enkephalin family (Schwarzer, 2009), within the LS shows no pattern other than a small dense band of dynorphin mRNA expressing cells immediately ventral to the corpus callosum in the LSd. Cells expressing GRH mRNA, which has been linked to regulating food intake (Vance, 1990), were found in the ventrolateral LSi, whereas neurons labeled with substance P mRNA, known for its role in regulating pain perception (Graefe & Mohiuddin, 2022), were found rostrally in the LSi as well as in a dense band ventral to the dynorphin band in the LSd.

The LS also contains mRNA for steroid hormone receptors, specifically mineralocorticoid, androgen, and estrogen. Mineralocorticoid receptor mRNA was found concentrated in the LSd and distributed similarly to LSd somatostatinergic neurons. These receptors are typically expressed in brain regions associated with affect, learning, memory, and HPA axis regulation (Gomez-Sanchez, 2014). Androgen receptor mRNA is also widely expressed in LSd neurons with dense expression in caudal LSd; androgen receptor expression is sexually dimorphic and regulates sexual behaviors, especially in males (Lu et al., 1998). The Lsv also showed dense expression of mRNA for estrogen receptors, and estrogen modulates neurotransmitter systems to affect cognitive processes, especially DA-dependent processes (Almey et al., 2015; Risold & Swanson, 1997a). Furthermore, while the specific functions of the various neuropeptides and receptors acting in the LS have not been fully established, these stark differences in expression of various neuropeptides and neurotransmitter receptors along the LS hints at the possibility of different functional subclasses of LS neurons along its dorsoventral (DV) and rostrocaudal axes.

DV organization of the LS

The dorsocaudal, intermediate-rostral, and ventral compartments of the LS receive differential inputs from the hippocampal formation along a DV gradient, as described above (Risold & Swanson, 1997b). There is emerging consensus that dHPC and vHPC are functionally distinct (Fanselow & Dong, 2010). This indicates that the LS might also show functional differences along its DV axis, which could explain how the LS contributes to such a wide range of behaviors. Additionally, the dorsal and ventral subregions of the LS are thought to mutually inhibit each other to modulate behavioral outputs (Leroy et al., 2018; Oliveira et al., 2021).

Approach, avoidance, and aggression

The function of projections within the LS to downstream subcortical targets can be categorized as leading to either approach or avoidance of a stimulus. When grouped, the projections that originate dorsally within the LS mediate approach behaviors, whereas excitation of ventrally situated projections leads to avoidance and aggressive behaviors. The best studied of these approach LS circuits, the dCA3-dorsal LS-ventral tegmental area (VTA) pathway, is involved in reward-seeking (Luo et al., 2011; Yeates et al., 2022). When the dorsal LS is excited by the dCA3, LS GABAergic projection neurons disinhibit the local tonic inhibitory cells in the VTA to allow DA release (Cai & Tong, 2022; Luo et al., 2011). Another reward-related approach circuit is the LSd projection to the nucleus accumbens (NAc) is described by Jonsson et al., 2017. Chemogenetic inhibition of the LSd-NAc led to decreased NAc DA release. Thus, the LSd is thought to mediate the reward-induced rise in DA levels in the NAc (Jonsson 2017). In contrast LSv projections to vmH appear to regulate aggression (Leroy et al., 2018; Nelson & Trainor, 2007). This circuit involves excitation of the LSd by the dCA2, then inhibition of the LSv by the

LSd, which leads to disinhibition of the vmH (Leroy et al., 2018). Consequently, activation of LSv inhibits aggression, another type of approach behavior (Wong et al., 2016). The aforementioned hyperaggressive phenotype of septal rage occurs when the LSv is lesioned, removing the ability of the LSv to gate aggressive behaviors and promote avoidance (Potegal et al., 1981).

In addition to specific LS-subcortical circuits supporting a topographical approach-avoidance organization, Clemens & Brecht, 2021 performed electrophysiological recordings along the DV axis of the LS that found nepotism in kin and non-kin preferences. Behaviorally, rat pups prefer kin scents before reaching 2 weeks of age, whereupon they begin to prefer nonkin scents. LS cells found more dorsally responded to nonkin, whereas kin-responsive cells were located more ventrally. As the preference for nonkin swaps from kin, the kin-responsive cells become less active overall (Clemens & Brecht, 2021). Future work is needed to establish how these cells might specifically mediate approach of nonkin and avoidance of kin, but the nepotism described in this study supports the hypothesis that cells along the DV axis of the LS vary in their functional representation of social stimuli.

Reward

Initial studies of septal rage induced by septal lesions resulted in animals ceasing to engage in previously rewarding self-stimulation (Kishore & Desiraju, 1990). Direct stimulation of the LS itself is also reinforcing in rats (Kishore & Desiraju, 1990), and place cells in the LS respond preferentially in the location of a reward (Wirtshafter & Wilson, 2020). Recordings of LS neurons along the DV axis also show that LS neurons encode spatial, directional, and self-motion information in the context of navigating towards a reward (van der Veldt et al., 2021). Specifically, more dorsally positioned LS cells were found to significantly encode direction of the animal,

whereas more ventrally positioned LS cells significantly encoded velocity. These data indicate that the LS plays an important role in reward-processing in the brain. The LS-NAc and LS-VTA circuitry are each functionally implicated in reward approach behaviors, and these pathways are localized more dorsally in the LS (Jonsson et al., 2017; Luo et al., 2011). However, it is unclear whether more ventral LS subregions are involved in reward-seeking or consumption or if they modulate avoidance of reward. As with nepotopy, there might be functional differences in representation of reward along the DV axis of the LS.

Aims and results

The LS mediates a wide range of behaviors, but it remains unresolved how such a variety of behaviors can be functionally modulated by this one brain region. One contributing factor is thought to be the anatomical heterogeneity of the LS. In fact, certain functionally distinct, subregion specific circuits within the LS have been identified to support this hypothesis. In addition, the connectivity and cytoarchitecture patterns of LS neurons have been shown to exhibit topographical organization along the DV axis. This anatomical evidence supports the potential existence of functionally distinct subpopulations of neurons in the LS that differentially contribute to behavior, specifically reward behaviors.

In order to establish if there are functional differences in how reward-related variables are represented along the DV of the LS, we performed cellular resolution calcium imaging of dorsal, intermediate, and ventral LS subregions while mice performed on an operant behavioral task. We have acquired preliminary data that there are differences in how and when LS neurons respond to reward along the DV axis of the LS. While this will require further studies to increase the validity

of the dataset, our preliminary results do provide evidence to support the hypothesis of functionally distinct subregions within the LS.

Additionally, beyond the hippocampus, it is unclear whether there are differences in brain-wide inputs to various projection populations within the LS. One possibility is that different LS projection populations could receive distinct patterns of inputs which in turn could contribute to functional heterogeneity (Benavidez et al., 2021; Besnard & Leroy, 2022; Huda et al., 2020). Using a monosynaptic rabies tracing strategy, we identified how whole-brain inputs to various LS projection populations are distributed across the DV axis of the LS. Our anatomical tracing results showed no apparent differences in the proportion of neurons projecting to different LS projection populations that were topographically organized along the DV axis of the LS. This result supports the idea that the LS contains functional units which receive overlapping inputs and mediate distinct behavioral outcomes.

Results

LS projection populations receive largely overlapping brain-wide inputs.

To characterize the monosynaptic inputs to distinct LS projection populations, we implemented a monosynaptic rabies tracing strategy (Figure 2a) and WholeBrain software (Figure 3) in mice (Fürth et al., 2018).

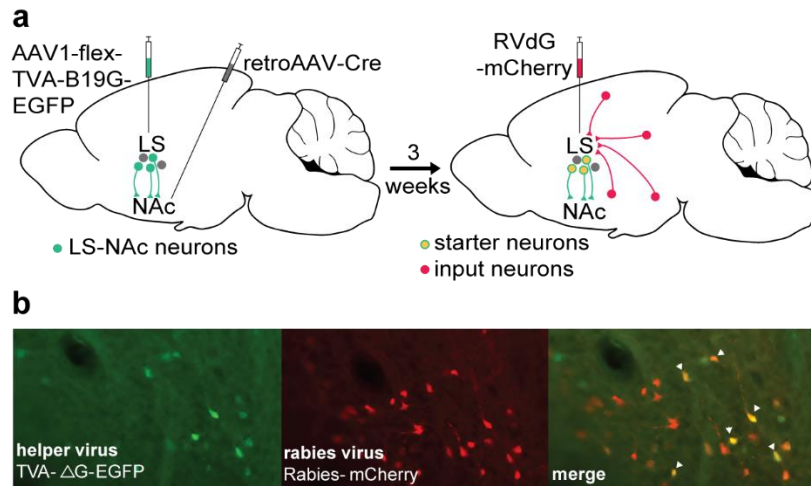


Figure 2. Monosynaptic rabies tracing. (a) Schematic of viral tracing strategy with the NAc as an example downstream target.

(b) LS neurons labeled with helper virus (green), rabies virus (red), and starter cells labeled with both (yellow).

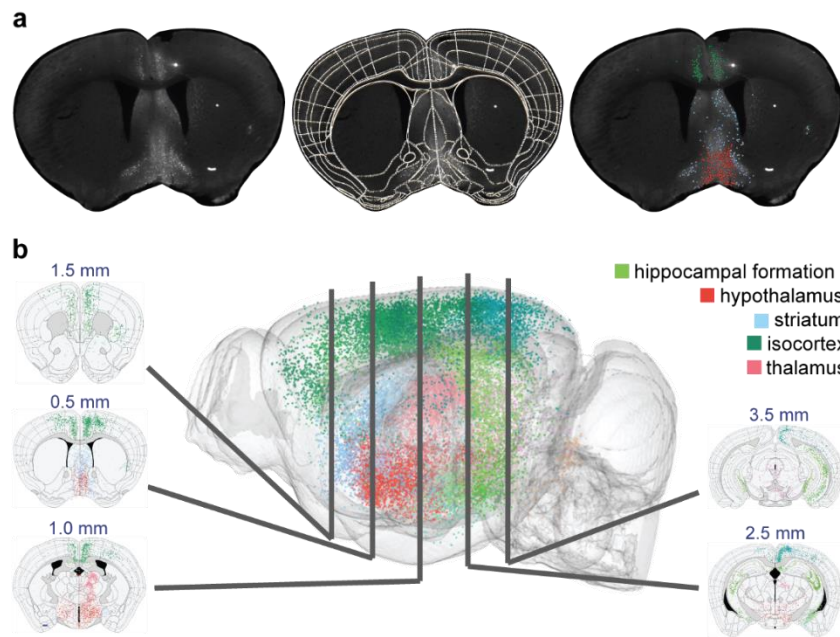


Figure 3. Wholebrain software analysis. (a) Original histology (left), segmentation of tissue (middle), and registered neurons (right).

(b) Example 3D model of brain-wide monosynaptic inputs to LS-NAc neurons with coronal slices labeled with AP distance from bregma. Each colored dot

represents an individual neuron. Each color represents a different brain region (see legend in figure).

We focused on LS projections to five major downstream target regions (Figure 4) implicated in a variety of social and reward behaviors (Deng et al., 2019). In particular we examined the connectivity patterns of the LS projection populations to the vmH (known for its role in aggression), the NAc (known for its role in reward-seeking), the VTA (known for its role in reward consumption), the basolateral amygdala or BLA (known for its role in anxiety and stress) and the bed nucleus of the stria terminalis or BNST (known for its role in context encoding and social avoidance) (Jonsson et al., 2017; Lebow & Chen, 2016; Luo et al., 2011; Nelson & Trainor, 2007; Sharp, 2017, p.).

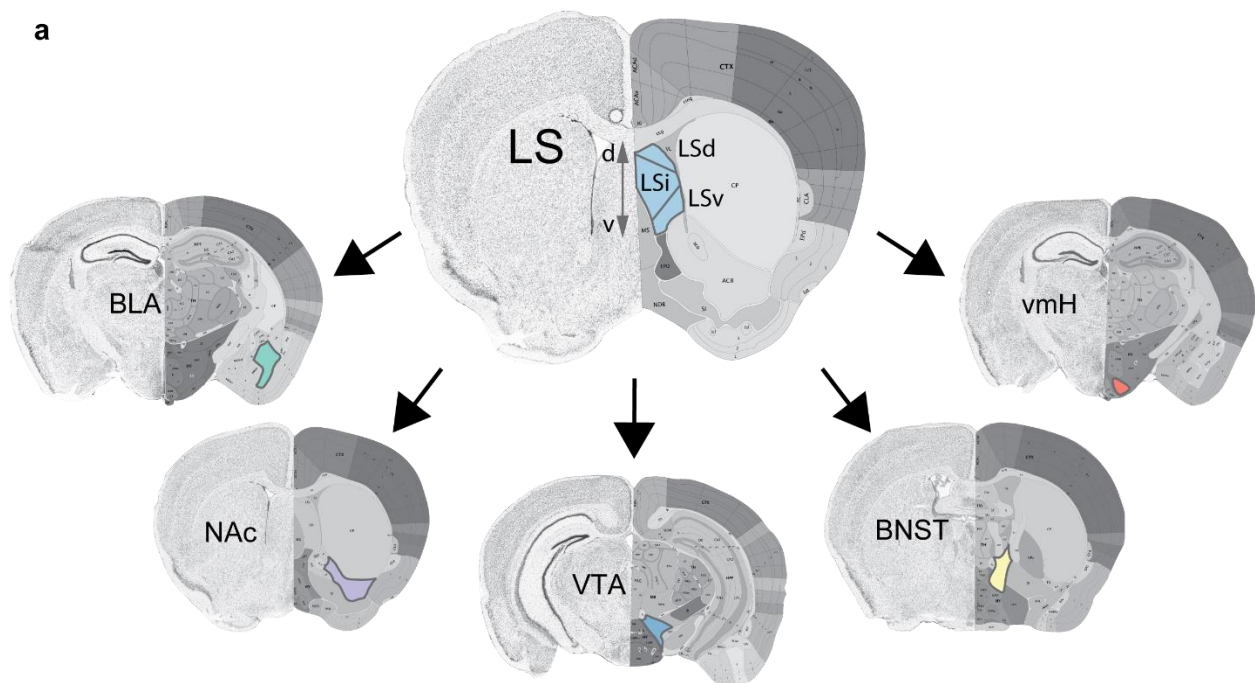


Figure 4. Anatomical locations of subcortical downstream targets of the LS. (a) The LS is known to project to the BLA, NAc, VTA, BNST, and vmH.

Using Wholebrain software (Figure 3), we analyzed the inputs to our 5 target projection populations across several animals (Figure 5). The LS-BLA projection (Figure 5a) had sparse inputs, totaling 3,410 input neurons from across the brain in a single animal. The LS-NAc and LS-VTA populations (Figure 5b) showed far denser bilateral inputs (Figure 5c), with each averaging approximately 30,000 input neurons per animal analyzed. The LS-BNST (Figure 5d) and LS-vmH (Figure 5e) projections each totaled 44,917 and 51,687 input neurons across 3 animals, or an average of 15,000 and 17,333 neurons per animal, respectively.

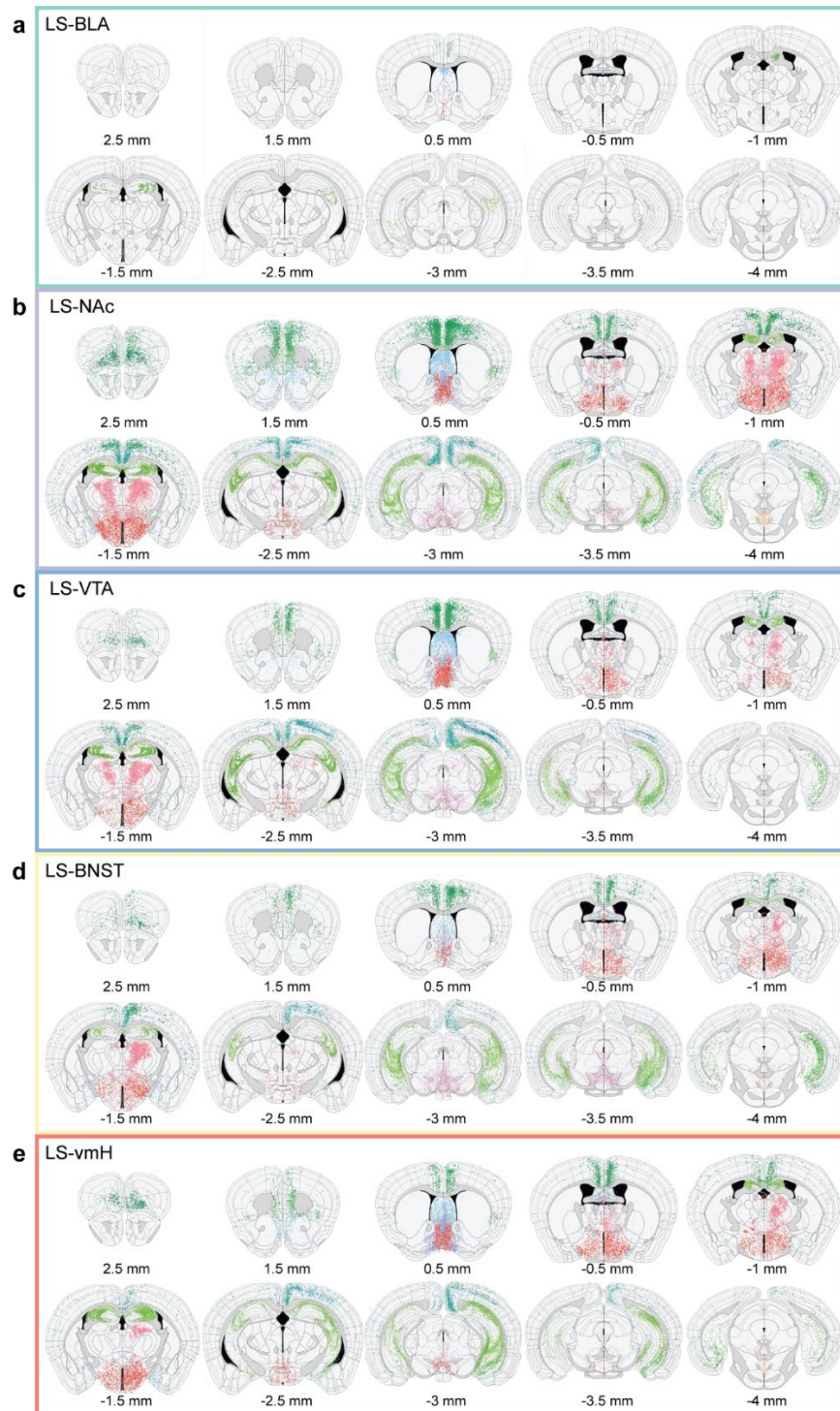


Figure 5. Distributions of monosynaptic inputs to LS projection populations. (a) Inputs to LS-BLA, 3410 neurons, $n = 1$. (b) Inputs to LS-NAc, 91738 neurons, $n = 3$. (c) Inputs to LS-VTA, 59199 neurons, $n = 2$. (d) Inputs to LS-BNST, 44917 neurons, $n = 3$. (e) Inputs to LS-vmH neurons, 51687 neurons, $n = 3$.

Coordinates relative to bregma.

In order to ascertain whether these inputs did vary by projection population, we quantified the results and identified the top input regions to each projection population (Figure 6a). We further examined the inputs from specific subregions within the hippocampal formation (Figure 6b), the hypothalamus (Figure 6c), and the thalamus (Figure 6d).

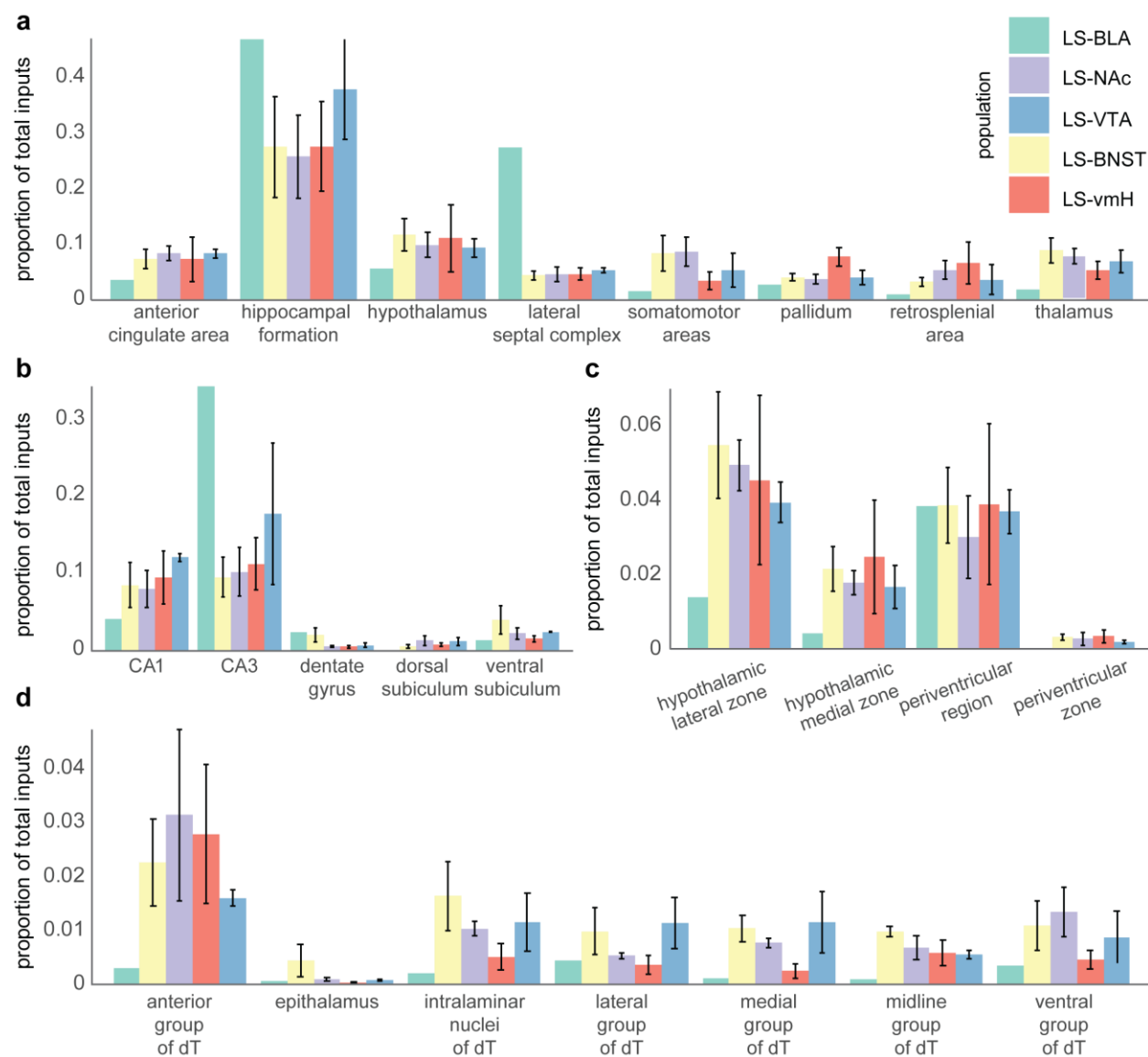


Figure 6. Quantification of monosynaptic inputs to LS projection populations. (a) Proportion of total input neurons from the top 8 input regions. (b) Proportion of total input neurons from the hippocampal formation. (c) Proportion of total input neurons from the hypothalamic subregions. (d) Proportion of total input neurons from dorsal thalamic (dT) subregions.

Starter cell populations occupy distinct compartments of the LS.

Though we found no differences in the regions sending inputs to the five LS projection populations, the starter cells for each population (Figure 2b) were consistently located in specific compartments within the LS (Figure 6a). LS-BLA cells were located anteromedially, just ventral to the corpus callosum. LS-NAc cells were also positioned just ventral to the corpus callosum, lateral to the LS-BLA cells. LS-VTA cells were found in the LSi. LS-BNST cells were in ventral LSi and LSv, directly adjacent to the medial septum. LS-vmH cells were even more ventral to LS-BNST cells and mostly in caudal LS.

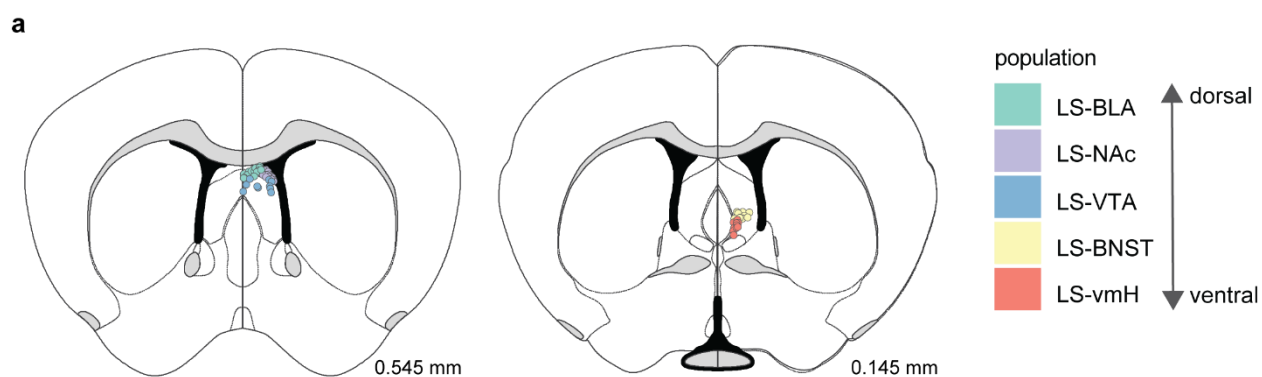


Figure 7. Representative starter cell locations along the DV axis of the LS. (a) The starter cells of each projection population show consistent topographical organization. LS-BLA starter cells are dorsomedial to the LS-NAc starter cells, which are dorsal to the LS-VTA starter cells. The LS-BNST and LS-vmH starter cells are both found more ventrally and caudally.

Both excitatory and inhibitory reward-responsive neurons are found along the LS DV axis.

To determine how reward responses are organized along the dorsoventral axis of the LS, we performed cellular resolution calcium imaging at varying depths in male mice (Figure 8). We implanted the GRIN lens at various depths targeting the LSd (-3.0mm), LSi (-3.2 mm), and LSV (-3.4mm) (Figure 8e).

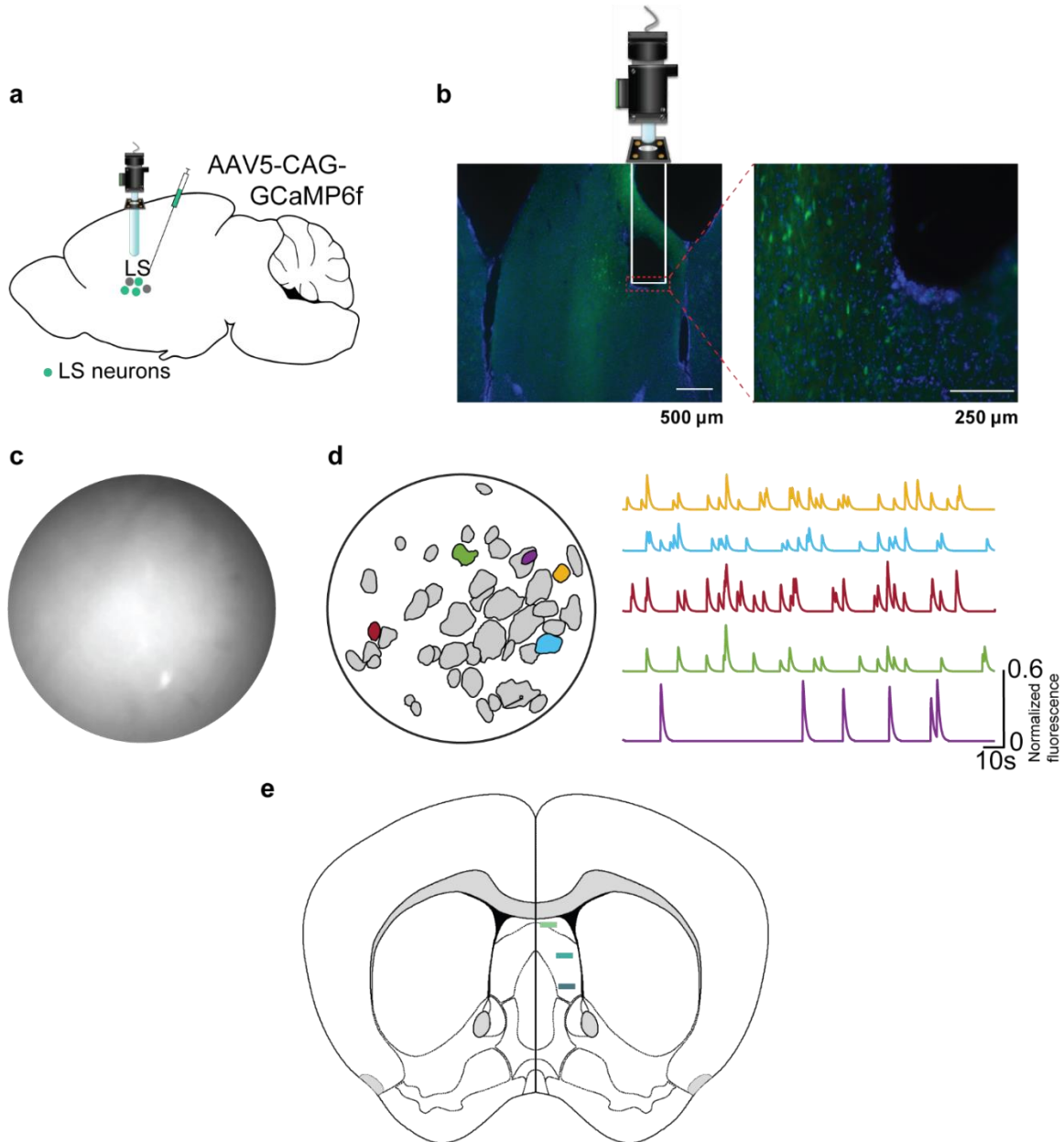


Figure 8. Cellular resolution calcium imaging. (a) Schematic of viral tracing strategy and lens implant. (b) Example histology of GRIN lens placement in the LS. (c) Example field of view (FOV) through a GRIN lens. (d) A reconstruction of the FOV with individual neurons identified using CNMFe. Example neurons and their fluorescence traces are highlighted. (e) Reconstruction of actual/expected GRIN lens placement in three animals using Wholebrain software: LSd in green, LSi in teal, LSv in blue. Coronal section 0.545 anterior to bregma.

Following the injection and implant, mice were group housed, placed on a restricted water access schedule (1.5 mL of water daily), and reverse light/dark cycle (lights off at 7am, lights on at 7pm). Their behavior was shaped through a series of progressively difficult operant assays in which they learned to associate illuminated ports with sucrose reward delivery. Mice were run on one hour daily sessions and were moved on to the next stage of training after reaching a predetermined number of successful pokes. In the operant conditioning paradigm (Figure 9a), mice were rewarded (10ul of 10% sucrose) for entering a reward port and reward port entry was marked by the illumination of the reward port. When an animal reached 50 pokes in a session, it progressed to the single port paradigm. In the single port assay, mice were trained to associate a nose port light with a reward (Figure 9b). Once the animal performed 40 successful nose-pokes in a session, it progressed to opposing port (Figure 9c). First, the port furthest from the reward port on the adjacent wall illuminates, and the mouse must first nose-poke this port before activating the reward port. Once the reward port illuminates, the mouse can retrieve its sucrose reward from the reward port.

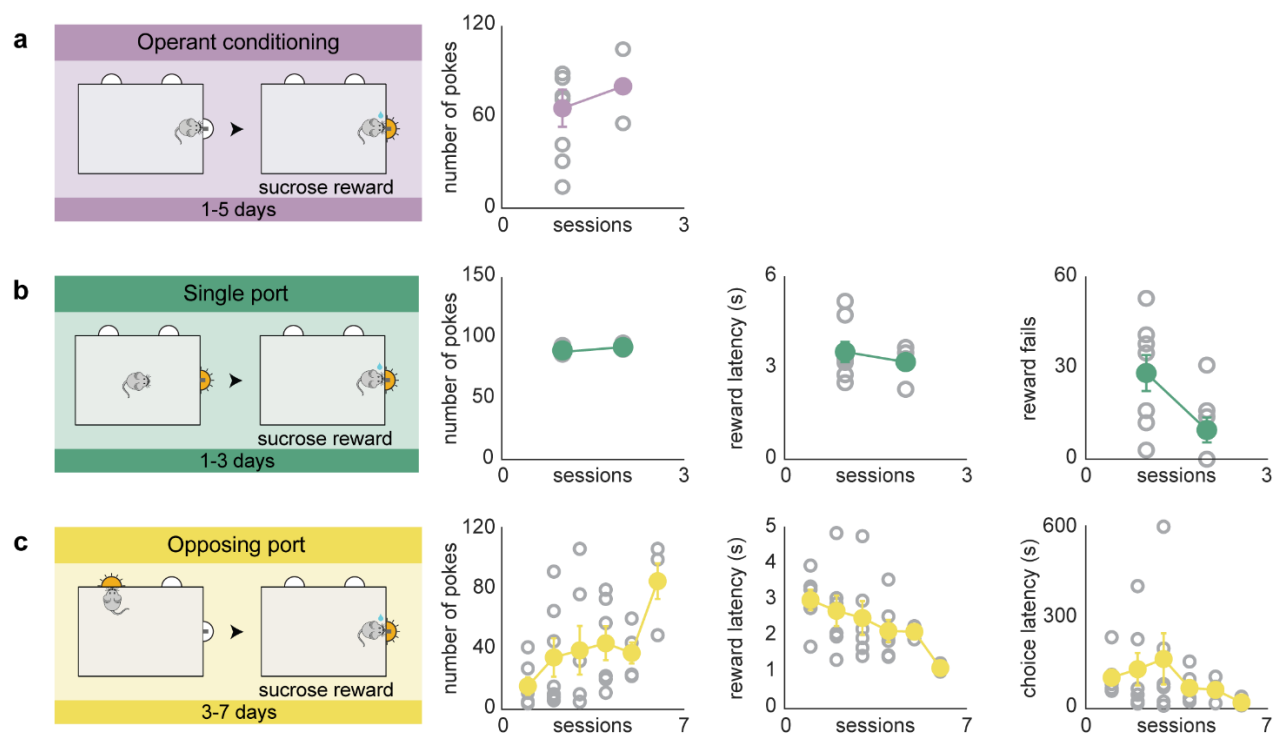


Figure 9. Behavioral paradigm and example results. (a) Mice are trained on a classical conditioning paradigm ($n = 5$) followed by (b) a single port paradigm ($n = 7$) where they must nose-poke the reward port after it illuminates. (c) Mice are then trained on opposing port, where a different port illuminates and the mouse must first nose-poke that port before the reward port illuminates, allowing the mouse to retrieve its sucrose reward. Representative behavioral results from 7 animals. Line plots show average behavioral outputs per session.

We collected imaging data from each behavioral session and analyzed the neural data from the final session of the opposing port paradigm for each animal (Figure 10). The majority of imaged neurons in each animal were responsive to reward (Figure 10g). In the LSd, 77% of the imaged neurons responded to reward port entry, and 54% of its neurons had an excitatory response. In the Lsv, 68% of the imaged neurons were responsive to reward and 49% had an

excitatory response. In contrast to the LSd and LSi, the imaged LSi neurons were 73% reward-responsive, but 44% of the total LSi neurons were inhibitory.

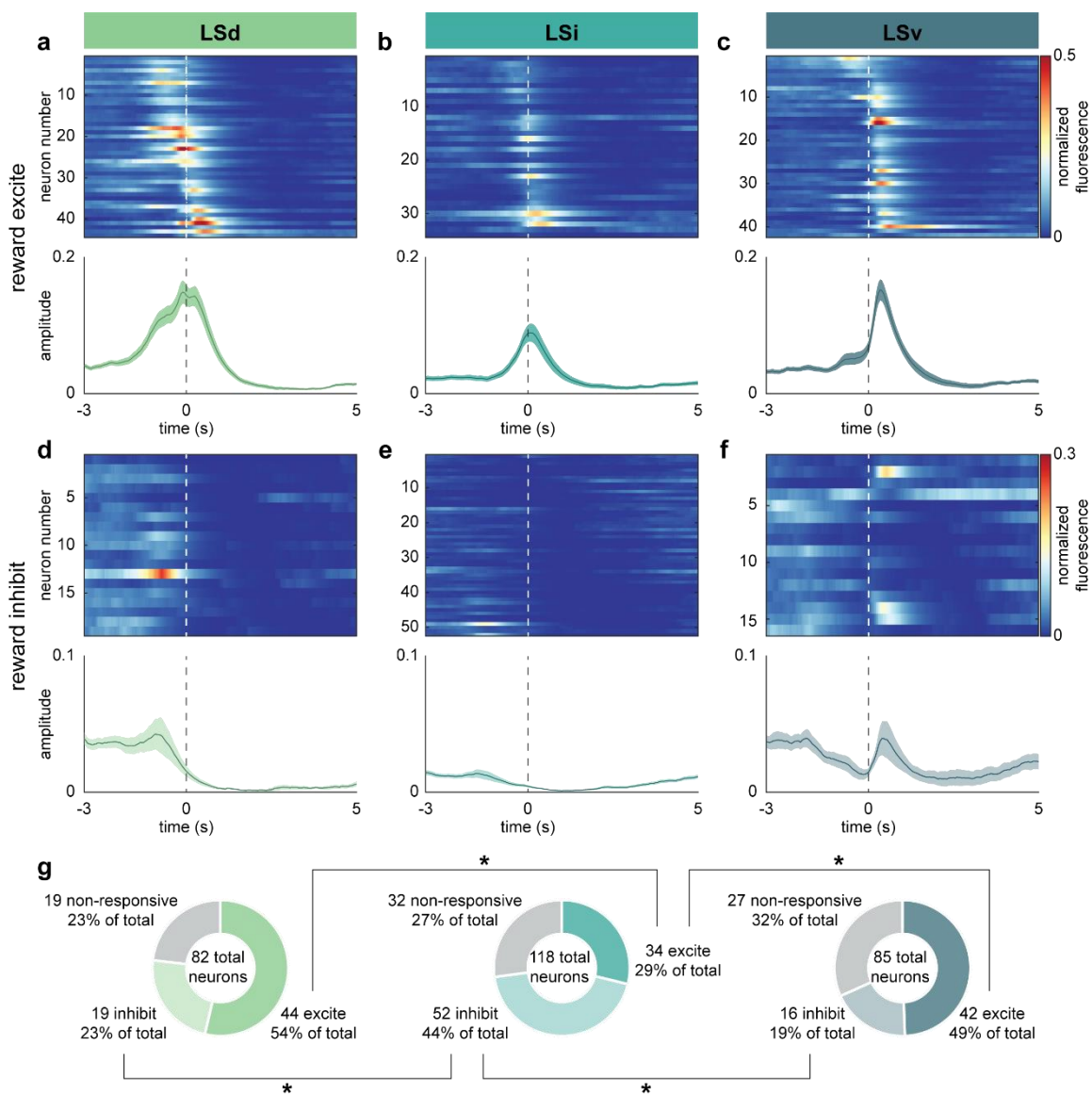


Figure 10. Time-locked excitatory and inhibitory reward-responses of LS neurons along the DV axis. (a, b, c) Heatmaps of neurons in the LSd (a), LSi (b), and LSi (c) that show an excitatory response to sucrose reward consumption (top panel) with the corresponding average fluorescence traces (bottom panel). (d, e, f) Heatmaps of neurons in the LSd (d), LSi (e), and LSi (f) that show an inhibitory response to sucrose reward consumption (top panel) with the corresponding average fluorescence traces (bottom panel). (g) The distribution of excitatory reward, inhibitory reward, and reward unresponsive neurons imaged from

each animal during the final day of opposing port. 2-proportion Z-test; excite - LSd-LSi: $p = 3.96 \times 10^{-4}$, LSd-LSv: $p = 0.583$, LSi-LSv: 2.80×10^{-3} ; inhibit - LSd-LSi: $p = 2.39 \times 10^{-3}$, LSd-LSv: $p = 0.490$, LSi-LSv: $p = 1.70 \times 10^{-4}$. Dashed line at zero indicates reward onset. Shaded region indicates \pm SE.

Excitatory reward-responsive neurons show varying temporal dynamics in the dorsal and ventral LS.

We next examined the excitatory reward-responsive neurons using a dimensionality reduction technique (Figure 11).

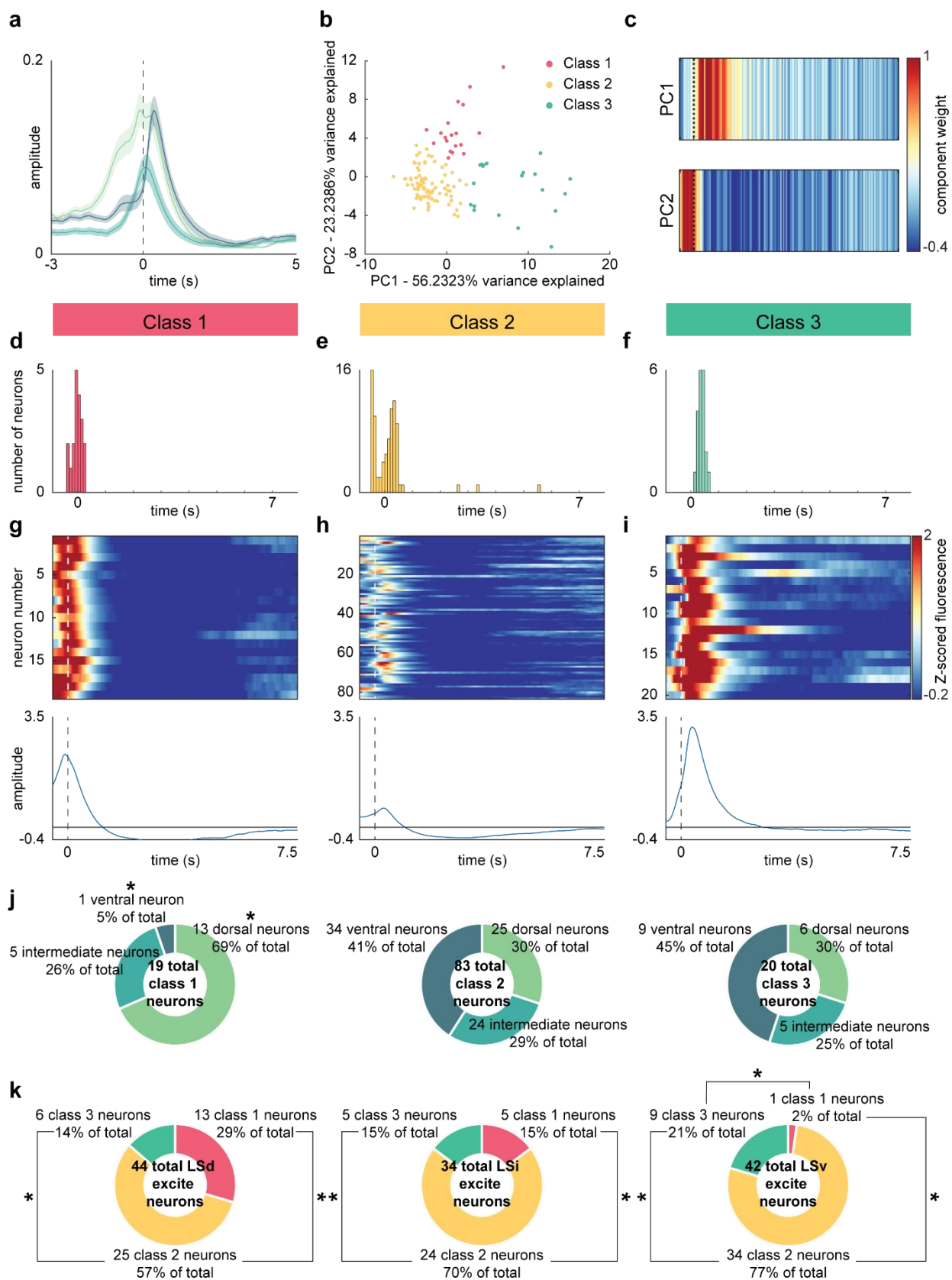


Figure 11. Temporal dynamics of excitatory reward responses in LSd, LSi, and LSv. (a) Overlay of average fluorescence traces (\pm SE) of excitatory reward responses in each animal aligned to reward port entry. LSd in green, LSi in teal, LSv in blue. (b) Principal component analysis (PCA) plot showing distribution of the three classes in the same state space. (c) Components of PCA plot that explain 79.4709% of variance in the dataset. (d) Class one neurons show mode peak amplitude of excitatory reward neurons 0.1 seconds before sucrose port entry. (e) Class two neurons show mode peak amplitude of excitatory reward neurons 0.3 seconds after sucrose port entry. (f) Class three neurons show mode peak amplitude of excitatory reward neurons 0.35 seconds after sucrose port entry. (g, h, i) Heatmaps of excitatory reward-responsive neurons within each class and corresponding average fluorescence traces with \pm SE both aligned to reward port entry. (j) Distribution of neurons within each class that came from the LSd, LSi, and LSv animals. 2-proportion Z-test; LSd - class one-class two: $p = 0.0018$, class one-class three: $p = 0.0164$, class two-class three: 0.99; LSi - class one-class two: $p = 0.821$, class one-class three: $p = 0.925$, class two-class three: 0.727; LSv - class one-class two: $p = 0.00311$, class one-class three: $p = 0.00450$, class two-class three: 0.742. (k) Distribution of neurons from each animal that contributed to class one, class two, and class three. 2-proportion Z-test; LSd - class one-class two: $p = 0.00981$, class one-class three: $p = 0.0697$, class two-class three: 2.23×10^{-5} ; LSi - class one-class two: $p = 3.18 \times 10^{-6}$, class one-class three: $p = 1$, class two-class three: 3.18×10^{-6} ; LSv - class one-class two: $p = 2.81 \times 10^{-13}$, class one-class three: $p = 0.00703$, class two-class three: 4.84×10^{-8} .

The average excited reward traces from the final day of opposing port from each animal, when overlaid, show a slight temporal difference (Figure 11a). We concatenated the neural data from excitatory reward-responsive neurons in the LSd, LSi, and LSv animals and performed a principal component analysis (PCA) (Figure 11b). Using this technique, three classes of responses were identified along two principal components (Figure 11c). The principal

components defining these classes also showed variance in temporal dynamics. Specifically, principal component one can explain ~56% of the variance in the dataset by identifying neurons that show peak response after the reward port entry (Figure 11b, c). Principal component two explains ~23% of the variance by identifying neurons that maximally respond at or before reward port entry. Each class that was identified was defined by the time of average peak response relative to reward port entry. Class one neurons responded immediately before and during reward port entry with the peak amplitude at 0.1 seconds before port entry (Figure 11d, g). Class two neurons show a far more reduced excitatory response with the peak amplitude of response coming 0.3 seconds after reward port entry (Figure 11e, h). Class three neurons responded almost exclusively at or immediately after reward port entry with the peak amplitude occurring 0.35 seconds after reward port entry (Figure 11f, i). Interestingly, a majority of the data contributing to class one came from the LSd, while the LSi contributed the least amount of data to class one relative to classes two and three (Figure 11j, k).

Activity of LS neurons differs on rewarded and unrewarded trials.

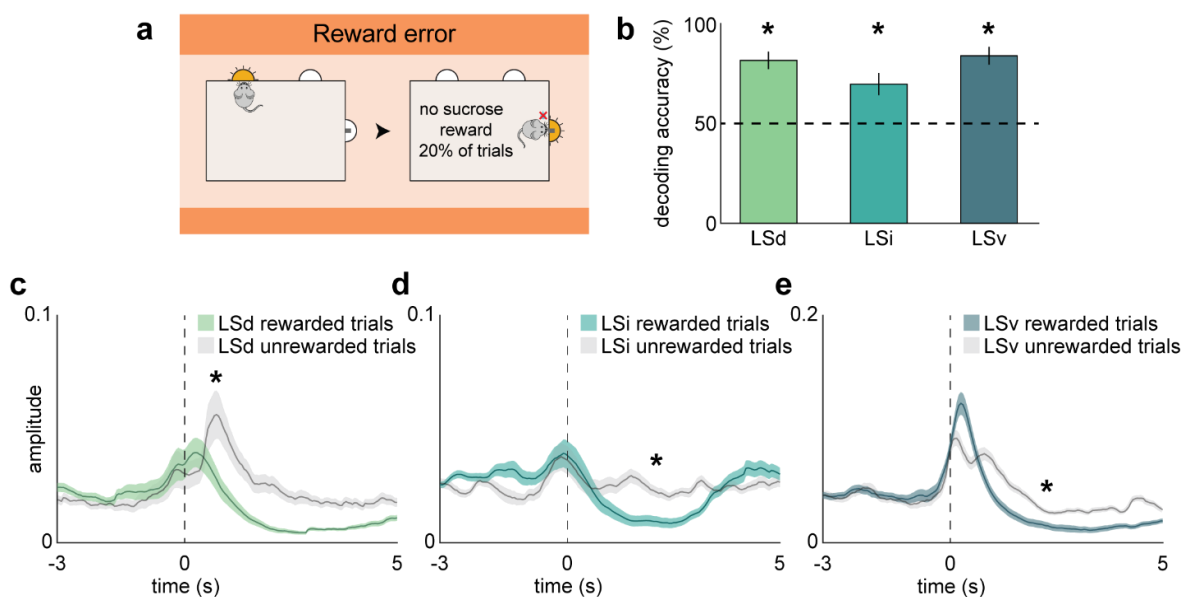


Figure 12. Decoding of neural activity on rewarded and unrewarded trials. (a) Mice are run on a reward error paradigm similar to the opposing port paradigm, except that sucrose reward delivery is withheld on a random 20% of trials following reward port activation. (b) Decoding of rewarded and unrewarded trials relative to chance (50%, indicated by dashed horizontal line) in the LSd (81.66 \pm 4.35), LSi (69.72 \pm 5.51), and LSv (83.96 \pm 4.50). Mean \pm SE. Wilcoxon rank sum test of mean compared to shuffled data; LSd: $p = 4.81 \times 10^{-67}$, LSi: $p = 1.73 \times 10^{-66}$, LSv: $p = 4.82 \times 10^{-67}$. (c, d, e) Average fluorescence traces from rewarded trials in green, teal, and blue from the LSd, LSi, and LSv animal respectively overlaid with the gray average traces from unrewarded trials. Mean peak amplitude of rewarded and unrewarded traces between 0-3s and unpaired t-test; LSd - mean rewarded: 0.0492, mean unrewarded: 0.0903, $p: 2.04 \times 10^{-5}$, LSi - mean rewarded: 0.0044, mean unrewarded: 0.0057, $p: 0.3116$, LSv - mean rewarded: 0.135, mean unrewarded: 0.127, $p: 0.304$. Mean minimum amplitude of rewarded and unrewarded traces between 0-3s and unpaired t-test; LSd - mean rewarded: 0.0025, mean unrewarded: 0.0039, $p: 0.118$, LSi - mean rewarded: 0.0457, mean unrewarded: 0.0599, $p: 5.82 \times 10^{-7}$, LSv - mean rewarded: 0.0072, mean unrewarded: 0.0128, $p: 0.0191$. Dashed line at zero indicates reward onset. Shaded region indicates \pm SE.

The final behavioral experiment was to determine if LS neurons encode a reward error. This paradigm is similar to the opposing port paradigm, except that the sucrose reward is not delivered on a random 20% of trials (Figure 12a). Whether a trial was rewarded or unrewarded can be decoded above chance (50%) from the activity of neurons in the LSd, LSi, and LSv (Figure 12b). The average fluorescence traces from rewarded and unrewarded trials in the LSd (Figure 12c), LSi (Figure 12d), and LSv (Figure 12e) show that rewarded and unrewarded trials are represented differently by LS neurons. The LSd has a significantly higher amplitude response within the 3 second window after reward port entry on unrewarded trials (Figure 12c). Unrewarded trials in the LSi appear to have a lack of inhibition after the reward response (Figure

12d). In the LSv, the amplitude of the response on rewarded trials is greater than the amplitude of the response on unrewarded trials (Figure 12e).

Discussion

In this study, using rabies tracing and whole brain mapping, we found that LS projection populations receive largely overlapping brain-wide monosynaptic inputs and that they occupy distinct subregions along the DV axis of the LS. Next, using cellular resolution calcium imaging during an operant paradigm, we found that LS reward-responsive neurons appear to represent reward differently depending on their location along the DV axis. Together, these results provide evidence to support the hypothesis of the LS functioning as a hub that intakes similar information from across the brain and transforms said information to modulate its downstream targets (Besnard & Leroy, 2022).

Anatomically positioned as a functional hub rather than relay station

Our rabies tracing confirmed earlier connectivity studies of the LS (Risold & Swanson, 1997b; Swanson & Cowan, 1979), but we were unable to find any differences in proportions of inputs to our target LS projection populations (Figure 6). However, we did find that our targeted LS projection populations can be localized in different areas along the DV axis (Figure 7). This evidence supports the hypothesis that the LS acts as a hub in the brain that also contains functional units, defined by Besnard and Leroy, 2022 as neurons in the LS that interact and project to a downstream region to modulate a specific behavioral output. These functional units could inhibit one another to shape a behavioral outcome or neuromodulators can act on functional units to affect an output. Because these units transform information rather than simply

acting as a relay for information to pass through unaltered, the information conveyed by similar inputs would be transformed in the LS as well. This would allow only relevant information to pass to the corresponding downstream regions from the LS to modulate distinct behaviors (Besnard & Leroy, 2022).

Temporal dynamics of LS reward responses along the DV axis

While we did find excitatory and inhibitory responses to reward consumption in each position along the DV axis (Figure 10) and differences in responses to rewarded and unrewarded trials (Figure 12), the most striking result from our pilot imaging study were the differences in the temporal dynamics in the activity patterns of the excitatory reward-responsive neurons (Figure 11). The LSd neurons contributed primarily to class one, which had the earliest response to reward port entry, whereas the LSv neurons strongly contributed to class three, which had the latest response to reward port entry. LSi neurons had an intermediate response. There are multiple possible explanations for this temporal variance.

First, as previously described, the most well-implicated subregions of the LS in reward responses are the LSd and LSi, as those compartments are known to project to the VTA and NAc (Rizzi-Wise & Wang, 2021). The LS-NAc and LS-VTA circuits have each been implicated in specific reward-related behaviors (Jonsson et al., 2017; Luo et al., 2011), and the NAc and VTA are each known to be a reward hub in the brain (Cai & Tong, 2022; G. Chen et al., 2023). However, the role of the LSv in responding to reward port entry is unclear. As we do see a response to reward port entry in the LSv, it is possible that a LSv circuit exists to convey reward-related information to another downstream target, and more studies will be required to identify this target and the nature of the connection. Additionally, our evidence of temporal variance

along the DV axis could involve the local LS circuitry. A previous study involving aggression has confirmed the presence of lateral inhibition in the LS between LS compartments (Leroy et al., 2018). That is, the LSd can inhibit the LSv. This intraseptal circuitry could explain the slight time delay between neural responses along the axis (Figure 11a), as information might be received within the LSd, then sent to the LSi and LSv. Future studies are needed to establish how this information is being transmitted within the LS and which neuromodulators might be involved.

Lateral inhibition

The concept of lateral inhibition in the LS is that it allows one behavior and its circuit to be promoted while a conflicting behavior is suppressed (Besnard & Leroy, 2022). A recent LS review puts forward a potential example of this: hungry mice show decreased territorial aggression in the presence of food (Besnard & Leroy, 2022; Burnett et al., 2019). In this situation, the review hypothesizes that an LS circuit involved in feeding could inhibit a circuit involved in aggression. Previous studies have shown control of hedonic feeding by neurotensin LS cells, which are primarily found in the LSi (Z. Chen et al., 2022; Risold & Swanson, 1997a), and that activation of GABA receptors in the LSi can stimulate feeding behavior (Gabiella et al., 2022). The subcircuits involved in feeding are found in LSi, while the role of the LSv in regulating aggression is well-established (Leroy et al., 2018; Potegal et al., 1981; Wong et al., 2016). The localization of each behavior to a distinct compartment allows for the possibility of lateral inhibition. If the temporal dynamics across the LS compartments when responding to reward (Figure 11) can be confirmed with an increased sample, lateral inhibition could provide a possible functional explanation of reward-related information being sent down the entire DV

axis, even to a LS compartment that has thus far not been implicated in reward-seeking or consumption.

Limitations and future directions

As genetic tools further develop, we acquire the ability to become more precise in our targeting to better parse out the potential function of circuits. In both our tracing and imaging experiments, we do not know the identity of the cells being labeled. The tracing experiments can define inputs to specific regions of the brain, but it is unknown what information these input cells are contributing to the projection population. Our next steps for analyzing this anatomical dataset will be to incorporate the axes of the input regions to determine whether there is topographical organization of inputs by a gradient rather than subregion. In the case of the imaging experiments, we are imaging only general LS cells along the DV axis. Though we can identify whether a response was excitatory or inhibitory in nature, we cannot describe to where these neurons project or their connectivity within a specific circuit. In addition, our cellular resolution imaging was designed as a pilot experiment, so we had only one animal per LS area. These experiments will be expanded on in the future as we add animals to our sample. Also, we plan to target specific projection neurons in our future imaging experiments, such as LS-VTA neurons, as well as specific cell types, such as dopaminergic projection neurons stemming from the LS.

Optogenetics is also a powerful tool for better understanding the role of regions and circuits in behavioral outputs (Emiliani et al., 2022). As we improve our understanding of the local LS circuitry and its associated projections to downstream regions, we can identify when to disrupt the neural activity associated with a behavior to find evidence to support the role of the region or circuit. Furthermore, the LS is known to play a role in many social behaviors, as

described above, but the question of social reward representation in the LS is yet to be addressed (Menon et al., 2022). In a novel operant task developed by the Murugan lab, the neural representation of social and nonsocial reward can be directly compared in the brain (Isaac et al., 2023). As we have found temporal differences in the representation of a nonsocial sucrose reward along the LS DV axis, this task would allow us to ascertain whether social reward representation also shows similar differences. If not, this could indicate a differential pathway for processing social reward in the LS.

Lastly, previous work in our lab has demonstrated that neural representations of reward in the LS_i can change over the course of training. The primary way that the neural representations change is recruitment of neurons to a response. However, we currently do not know where these neurons are recruited from: whether they were previously non-responsive or responsive to a different aspect of the task. Implementation of a cell tracking method would allow us to parse out the identities of the recruited neurons to better understand the role of the LS in learning and memory of a task, as well as the plasticity of the LS (Sheintuch et al., 2017).

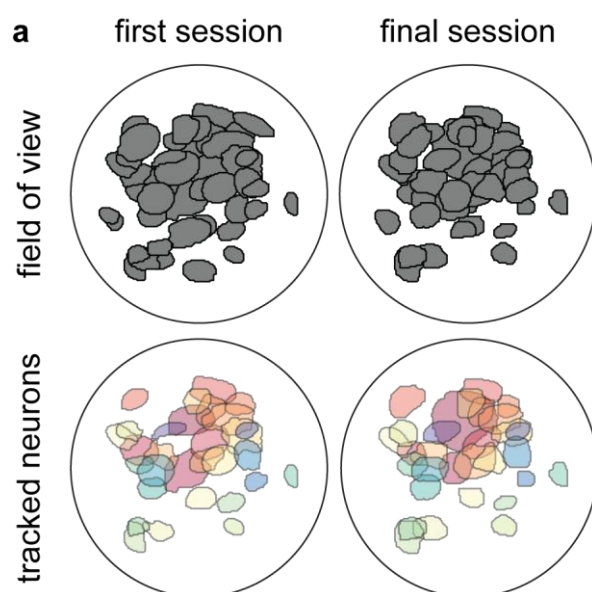


Figure 12. Tracking neurons across training. (a) Top panel shows LS field of view on first (left) and final (right) days of training on the opposing port stage. Bottom panel shows LS neurons that were tracked across imaging sessions. Individual neurons are shown in different colors.

Methods

Experimental subjects

For all experiments, we used C57BL/6J male mice aged 6-10 weeks from Jackson laboratories. Calcium imaging mice were maintained on a reverse light dark cycle (lights off at 7am, lights on at 7pm). All procedures were approved by the Emory Institutional Animal Care and Use Committee.

Viruses

The viruses used were purchased from Addgene:

AAV1-flex-TVA-B19G-EGFP

retroAAV-Cre

RVdG-mCherry

AAV5-Syn-GCaMP6f-WPRE-SV40 (100835-AAV5).

Stereotaxic surgeries

For tracing surgeries, mice aged ~6-8 weeks (n = 12 mice) were anesthetized with 1-2% isoflurane and placed in stereotactic setup (Kopf). A microsyringe (Nanoject) was used to inject 0.75 μ L of AAV1-flex-TVA-B19G-EGFP unilaterally into the lateral septum (0 mm anterior, 0.4 mm lateral, and 2.8 mm in depth) and 0.75 μ L of retroAAV-Cre into a target downstream region

within the same hemisphere. After 3 weeks, 0.50 μ L of RVdG-mCherry was injected in the lateral septum using the same coordinates (Figure 2a).

For imaging surgeries, mice aged ~6-8 weeks ($n = 3$ mice) were anesthetized with 1-2% isoflurane and placed in stereotactic setup. A microsyringe was used to inject 0.75 μ L of AAV5-Syn-GCaMP6f-WPRE-SV40 unilaterally into either the dorsal (0 mm anterior, 0.4 mm lateral and 2.8 mm in depth), intermediate (0 mm anterior, 0.4 mm lateral, 3.0 mm in depth), ventral (0 mm anterior, 0.45 mm lateral and -3.2 mm in depth) LS. Mice were then implanted with a 0.5 mm diameter, 6.1 mm length GRIN lens in the corresponding compartment of the LS (dorsal: 0.5 mm, 0.4 mm, -3.0 mm, intermediate: 0.5 mm, 0.4 mm, -3.2 mm, ventral: 0.3 mm, 0.45 mm, -3.4 mm) (Figure8b). A metal cap was cemented over the lens to protect it. Mice were group housed following lens implant. 3-4 weeks following viral injection and lens implant, a baseplate attached to the miniature microscope was positioned ~0.45 mm above the lens such that blood vessels and neurons were in focus. The baseplate was then cemented in place using dental cement, and a baseplate cover was used to protect the lens.

Whole-brain anatomical analysis

Using the open-source Wholebrain R package (Fürth et al., 2018), we registered each imaged section of the brains injected with the modified rabies virus (Figure 3a) by overlaying the corresponding regions drawn from the standardized Allen Brain Atlas (*Atlas Thumbnails :: Allen Brain Atlas: Mouse Brain*, n.d.). The coronal section taken from the atlas was manually decided using anatomical markers in the tissue. The registered image was then segmented using a filter for soma size and brightness designed to identify neurons tagged with mCherry. After the

neurons were automatically identified by the software, we performed manual addition and deletion of misidentified somas.

Behavioral assay

We generated an automated operant assay to quantitatively assess nonsocial reward behaviors. The assay consists of an acrylic chamber (12x12x12 inches) with three ports: one that delivers a 10% sucrose reward, one that allows the mouse to nose-poke for the sucrose reward, and one that acts as a “dummy” port, which does nothing (Figure 9). The choice and dummy ports are each three inches from the corners of the box, while the reward port is centered on the adjacent wall. Each port is one inch from the base of the chamber, and they detect a nose-poke when the infrared beam in the opening of the port is broken. Mice are trained on the assay and progress through each training stage as they meet certain poke thresholds (Figure 9).

Training and behavioral paradigms

Mice were co-housed and placed on a restricted water schedule prior to the start of training. At the end of each day mice were provided 1.5 mL of water in addition to their consumption during training.

Operant conditioning

The LED in the reward port would light at the start of the trial, indicating the mouse can poke for a sucrose reward of 10 μ L of 10% sucrose in water. Once the mouse nose-pokes, the LED turns off and the mouse receives its sucrose reward. After 15 seconds, the next trial begins, and the mouse can poke again for a reward. The mice were required to perform a minimum of 50 pokes

in a single session to continue to the next stage of training. Each session lasted one hour, and animals ran on the assay once a day. If the animal did not engage with the reward port for more than two minutes after the start of the trial, then the reward port delivered 30 μ L liquid without engaging the LED. This automatic reward delivery also occurred at the beginning of the first trial in each session to prime the animal to engage with the port.

Single port

The LED in the reward port would light at the start of the trial, and the mouse would have 8s to poke the port to receive 10 μ L of sucrose water. The intertrial interval was 30s, and the animal needed to wait 3s before entering the port for the next trial to begin. A trial was considered a reward fail if the mouse failed to enter the reward port after the 8s period. Mice had to achieve a minimum of 40 successful trials during one hour-long session to advance to the next training stage.

Opposing port

In the third stage, the choice port LED turned on to indicate the trial start. A successful choice port poke resulted in the LED flashing on and off successively 3 times in 0.1s intervals, after which the reward port LED turned on for up to 8s. Mice had to nose-poke the reward port within this window to receive a 10 μ L sucrose reward. Failure to do so resulted in a reward fail and initiation of a new trial. Trials were separated by a 15s ITI. In addition, if the animal engaged with the dummy port instead of the choice port during the choice period, the current trial ended. Mice had to refrain from entering the choice port for 3s in order for the next trial to start. Mice had to perform 40 successful sucrose reward trials to proceed to the next stage.

Reward error

The reward error stage functions similarly to opposing port, but when a mouse performs a successful trial, 20% of the trials will be unrewarded (Figure 12a). The mouse must nose-poke the lit up choice port, then reach the lighted reward port within 8 seconds, and on a randomly selected 20% of trials, the reward port will not dispense a sucrose reward. The reward port LED does turn off when the mouse enters the reward port.

Behavioral analysis

All behavioral sessions were recorded at 40 Hz using Pylon software. Several metrics were used to quantify mouse behavior for a given behavioral session, including number of pokes, choice latency and reward latency. Poke number was defined as the total number of times that an animal nose-poked the choice port, independent of reward consumption. Number of poke fails was determined as the total number of times that an animal nose-poked the choice port and failed to reach the reward port when the reward was available for consumption. Choice latency was defined as the time between when the choice port LED turned on (trial start) and the animal nose-poked the choice port. Reward latency was defined as the time from the start of the presentation of the reward, when the mouse nose-pokes the choice port, to the consumption of the reward, when the mouse enters the reward port.

Endoscopic calcium imaging experiments and analysis

After completion of the stereotaxic surgery, the implanted mice were run sequentially through the training and behavioral paradigms. During each session, mice were imaged with the Inscopix

nVista single-channel miniscope. The LED power was set to 0.7, and the analog gain on the image sensor was set to 1.6-1.8. The video was captured at 20 Hz using Inscopix nVista software. Following imaging acquisition, data were spatially downsampled by a factor of 4 and motion corrected using Inscopix software.

Once the mice had been trained for ~2 weeks, they were implanted with the baseplate and habituated with a tethered dummy microscope (Product ID: 1050-003762, Inscopix) during behavioral sessions for at least 3 days prior to the actual imaging session. On the day of imaging, mice were allowed to habituate to the scope for 10 minutes prior to the start of the session. During the behavioral imaging session, the LED power was set to 0.7 and the analog gain on the image sensor was set to 1.6-1.8. Images were acquired at 20 Hz using Inscopix nVista software. Following imaging acquisition, data were spatially downsampled by a factor of 4 and motion corrected using Inscopix software. A CNMFe algorithm was then used to identify individual neurons and their fluorescence traces (Zhou et al., 2018). The fluorescence traces were subsequently aligned to the behavioral data and used for task modulation analysis. Custom MATLAB software was used for all imaging data analysis.

Histology and microscopy

After all anatomical tracing and imaging experiments were completed, mice were sacrificed and perfused with 0.5% PBS followed by 4% paraformaldehyde. The brains were dissected out and fixed in 4% PFA overnight at 4°F. They were then transferred to 30% sucrose solution and allowed to fix for a minimum of 24 hours. To visualize viral expression and GRIN lens placement, brains were sliced at 50µm slices using an Eprexia HM430 microtome. Every other

slice of the whole brain anatomical tracing experiments was mounted with DAPI solution, while all slices containing the lateral septum from the calcium imaging experiments were mounted. Slices were imaged using fluorescence microscopy. Images were registered using WholeBrain software to quantify cells labeled by rabies virus or to determine GRIN lens placement.

References

- Albert, D. J., & Chew, G. L. (1980). *The Septal Forebrain and the Inhibitory Modulation of Attack and Defense in the Rat. A Review I.*
- Almey, A., Milner, T. A., & Brake, W. G. (2015). Estrogen receptors in the central nervous system and their implication for dopamine-dependent cognition in females. *Hormones and Behavior, 74*, 125–138. <https://doi.org/10.1016/j.yhbeh.2015.06.010>
- Atlas Thumbnails: Allen Brain Atlas: Mouse Brain.* (n.d.). Retrieved March 24, 2023, from https://mouse.brain-map.org/experiment/thumbnails/100048576?image_type=atlas
- Benavidez, N. L., Bienkowski, M. S., Zhu, M., Garcia, L. H., Fayzullina, M., Gao, L., Bowman, I., Gou, L., Khanjani, N., Cotter, K. R., Korobkova, L., Becerra, M., Cao, C., Song, M. Y., Zhang, B., Yamashita, S., Tugangui, A. J., Zingg, B., Rose, K., ... Dong, H.-W. (2021). Organization of the inputs and outputs of the mouse superior colliculus. *Nature Communications, 12*(1), Article 1. <https://doi.org/10.1038/s41467-021-24241-2>
- Besnard, A., & Leroy, F. (2022). Top-down regulation of motivated behaviors via lateral septum sub-circuits. *Molecular Psychiatry, 1*–10. <https://doi.org/10.1038/s41380-022-01599-3>
- Boules, M., Li, Z., Smith, K., Fredrickson, P., & Richelson, E. (2013). Diverse Roles of Neurotensin Agonists in the Central Nervous System. *Frontiers in Endocrinology, 4*, 36. <https://doi.org/10.3389/fendo.2013.00036>
- Burnett, C. J., Funderburk, S. C., Navarrete, J., Sabol, A., Liang-Guallpa, J., Desrochers, T. M., & Krashes, M. J. (2019). Need-based prioritization of behavior. *ELife, 8*, e44527. <https://doi.org/10.7554/eLife.44527>

- Cai, J., & Tong, Q. (2022). Anatomy and Function of Ventral Tegmental Area Glutamate Neurons. *Frontiers in Neural Circuits*, *16*, 867053.
<https://doi.org/10.3389/fncir.2022.867053>
- Chen, G., Lai, S., Bao, G., Ke, J., Meng, X., Lu, S., Wu, X., Xu, H., Wu, F., Xu, Y., Xu, F., Bi, G.-Q., Peng, G., Zhou, K., & Zhu, Y. (2023). Distinct reward processing by subregions of the nucleus accumbens. *Cell Reports*, *42*(2). <https://doi.org/10.1016/j.celrep.2023.112069>
- Chen, Z., Chen, G., Zhong, J., Jiang, S., Lai, S., Xu, H., Deng, X., Li, F., Lu, S., Zhou, K., Li, C., Liu, Z., Zhang, X., & Zhu, Y. (2022). A circuit from lateral septum neurotensin neurons to tuberal nucleus controls hedonic feeding. *Molecular Psychiatry*, *27*(12), Article 12.
<https://doi.org/10.1038/s41380-022-01742-0>
- Clemens, A. M., & Brecht, M. (2021). Neural representations of kinship. *Current Opinion in Neurobiology*, *68*, 116–123. <https://doi.org/10.1016/j.conb.2021.02.007>
- Clemens, A. M., Wang, H., & Brecht, M. (2020). The lateral septum mediates kinship behavior in the rat. *Nature Communications*, *11*(1), Article 1. <https://doi.org/10.1038/s41467-020-16489-x>
- Deng, K., Yang, L., Xie, J., Tang, H., Wu, G.-S., & Luo, H.-R. (2019). Whole-brain mapping of projection from mouse lateral septal nucleus. *Biology Open*, *8*(7), bio043554.
<https://doi.org/10.1242/bio.043554>
- Emiliani, V., Entcheva, E., Hedrich, R., Hegemann, P., Konrad, K. R., Lüscher, C., Mahn, M., Pan, Z.-H., Sims, R. R., Vierock, J., & Yizhar, O. (2022). Optogenetics for light control of biological systems. *Nature Reviews Methods Primers*, *2*(1), Article 1.
<https://doi.org/10.1038/s43586-022-00136-4>

- Fanselow, M. S., & Dong, H.-W. (2010). Are The Dorsal and Ventral Hippocampus functionally distinct structures? *Neuron*, *65*(1), 7. <https://doi.org/10.1016/j.neuron.2009.11.031>
- Fürth, D., Vaissière, T., Tzortzi, O., Xuan, Y., Martin, A., Lazaridis, I., Spigolon, G., Fisone, G., Tomer, R., Deisseroth, K., Carlén, M., Miller, C. A., Rumbaugh, G., & Meletis, K. (2018). An interactive framework for whole-brain maps at cellular resolution. *Nature Neuroscience*, *21*(1), Article 1. <https://doi.org/10.1038/s41593-017-0027-7>
- Gabriella, I., Tseng, A., Sanchez, K. O., Shah, H., & Stanley, B. G. (2022). Stimulation of GABA Receptors in the Lateral Septum Rapidly Elicits Food Intake and Mediates Natural Feeding. *Brain Sciences*, *12*(7), 848. <https://doi.org/10.3390/brainsci12070848>
- Gomez-Sanchez, E. (2014). Brain mineralocorticoid receptors in cognition and cardiovascular homeostasis. *Steroids*, *91*, 20–31. <https://doi.org/10.1016/j.steroids.2014.08.014>
- Graefe, S. B., & Mohiuddin, S. S. (2022). Biochemistry, Substance P. In *StatPearls*. StatPearls Publishing. <http://www.ncbi.nlm.nih.gov/books/NBK554583/>
- Guo, Z., Yin, L., Osakada, T., Lischinsky, J., Chien, J., Dai, B., Urtecho, A., Tong, X., Chen, Z. S., & Lin, D. (2023). *Neural dynamics in the limbic system during male social behaviors* (p. 2023.03.12.532199). bioRxiv. <https://doi.org/10.1101/2023.03.12.532199>
- Huda, R., Sipe, G. O., Breton-Provencher, V., Cruz, K. G., Pho, G. N., Adam, E., Gunter, L. M., Sullins, A., Wickersham, I. R., & Sur, M. (2020). Distinct prefrontal top-down circuits differentially modulate sensorimotor behavior. *Nature Communications*, *11*, 6007. <https://doi.org/10.1038/s41467-020-19772-z>
- Isaac, J., Karkare, S., Balasubramanian, H., Schappagh, N., Javier, J., Rashid, M., & Murugan, M. (2023). *Sex differences in neural representations of social and nonsocial reward in*

the medial prefrontal cortex (p. 2023.03.09.531947). bioRxiv.

<https://doi.org/10.1101/2023.03.09.531947>

- Jonsson, S., Morud, J., Stomberg, R., Ericson, M., & Söderpalm, B. (2017). Involvement of lateral septum in alcohol's dopamine-elevating effect in the rat. *Addiction Biology*, 22(1), 93–102. <https://doi.org/10.1111/adb.12297>
- Kishore, K. R., & Desiraju, T. (1990). Inhibition of positively rewarding behavior by the heightened aggressive state evoked either by pain-inducing stimulus or septal lesion. *Indian Journal of Physiology and Pharmacology*, 34(2), 125–129.
- Kondo, Y., Shinoda, A., Yamanouchi, K., & Arai, Y. (1990). Role of septum and preoptic area in regulating masculine and feminine sexual behavior in male rats. *Hormones and Behavior*, 24(3), 421–434. [https://doi.org/10.1016/0018-506x\(90\)90019-t](https://doi.org/10.1016/0018-506x(90)90019-t)
- Lebow, M. A., & Chen, A. (2016). Overshadowed by the amygdala: The bed nucleus of the stria terminalis emerges as key to psychiatric disorders. *Molecular Psychiatry*, 21(4), Article 4. <https://doi.org/10.1038/mp.2016.1>
- Leroy, F., Park, J., Asok, A., Brann, D. H., Meira, T., Boyle, L. M., Buss, E. W., Kandel, E. R., & Siegelbaum, S. A. (2018). A circuit from hippocampal CA2 to lateral septum disinhibits social aggression. *Nature*, 564(7735), Article 7735. <https://doi.org/10.1038/s41586-018-0772-0>
- Leutgeb, S., & Mizumori, S. J. Y. (1999). Excitotoxic Septal Lesions Result in Spatial Memory Deficits and Altered Flexibility of Hippocampal Single-Unit Representations. *The Journal of Neuroscience*, 19(15), 6661–6672. <https://doi.org/10.1523/JNEUROSCI.19-15-06661.1999>

- Lu, S., McKenna, S. E., Cologer-Clifford, A., Nau, E. A., & Simon, N. G. (1998). Androgen Receptor in Mouse Brain: Sex Differences and Similarities in Autoregulation*. *Endocrinology*, *139*(4), 1594–1601. <https://doi.org/10.1210/endo.139.4.5863>
- Luo, A. H., Tahsili-Fahadan, P., Wise, R. A., Lupica, C. R., & Aston-Jones, G. (2011). Linking Context with Reward: A Functional Circuit from Hippocampal CA3 to Ventral Tegmental Area. *Science (New York, N.Y.)*, *333*(6040), 353–357. <https://doi.org/10.1126/science.1204622>
- Menon, R., Süß, T., Oliveira, V. E. de M., Neumann, I. D., & Bludau, A. (2022). Neurobiology of the lateral septum: Regulation of social behavior. *Trends in Neurosciences*, *45*(1), 27–40. <https://doi.org/10.1016/j.tins.2021.10.010>
- Nelson, R. J., & Trainor, B. C. (2007). Neural mechanisms of aggression. *Nature Reviews Neuroscience*, *8*(7), Article 7. <https://doi.org/10.1038/nrn2174>
- Oliveira, V. E. de M., Lukas, M., Wolf, H. N., Durante, E., Lorenz, A., Mayer, A.-L., Bludau, A., Bosch, O. J., Grinevich, V., Egger, V., de Jong, T. R., & Neumann, I. D. (2021). Oxytocin and vasopressin within the ventral and dorsal lateral septum modulate aggression in female rats. *Nature Communications*, *12*(1), Article 1. <https://doi.org/10.1038/s41467-021-23064-5>
- Potegal, M., Blau, A., & Glusman, M. (1981). Effects of anteroventral septal lesions on intraspecific aggression in male hamsters. *Physiology & Behavior*, *26*(3), 407–412. [https://doi.org/10.1016/0031-9384\(81\)90167-0](https://doi.org/10.1016/0031-9384(81)90167-0)
- Risold, P. Y., & Swanson, L. W. (1996). Structural Evidence for Functional Domains in the Rat Hippocampus. *Science*, *272*(5267), 1484–1486. <https://doi.org/10.1126/science.272.5267.1484>

- Risold, P. Y., & Swanson, L. W. (1997a). Chemoarchitecture of the rat lateral septal nucleus¹Published on the World Wide Web on 2 June 1997.1. *Brain Research Reviews*, 24(2), 91–113. [https://doi.org/10.1016/S0165-0173\(97\)00008-8](https://doi.org/10.1016/S0165-0173(97)00008-8)
- Risold, P. Y., & Swanson, L. W. (1997b). Connections of the rat lateral septal complex¹Published on the World Wide Web on 2 June 1997.1. *Brain Research Reviews*, 24(2), 115–195. [https://doi.org/10.1016/S0165-0173\(97\)00009-X](https://doi.org/10.1016/S0165-0173(97)00009-X)
- Rizzi-Wise, C. A., & Wang, D. V. (2021). Putting Together Pieces of the Lateral Septum: Multifaceted Functions and Its Neural Pathways. *ENeuro*, 8(6). <https://doi.org/10.1523/ENEURO.0315-21.2021>
- Schnurr, R. (1972). Localization of the septal rage syndrome in Long-Evans rats. *Journal of Comparative and Physiological Psychology*, 81, 291–296. <https://doi.org/10.1037/h0033528>
- Schwarzer, C. (2009). 30 Years of Dynorphins – New Insights on Their Functions in Neuropsychiatric Diseases. *Pharmacology & Therapeutics*, 123(3), 353–370. <https://doi.org/10.1016/j.pharmthera.2009.05.006>
- Sharp, B. M. (2017). Basolateral amygdala and stress-induced hyperexcitability affect motivated behaviors and addiction. *Translational Psychiatry*, 7(8), Article 8. <https://doi.org/10.1038/tp.2017.161>
- Sheintuch, L., Rubin, A., Brande-Eilat, N., Geva, N., Sadeh, N., Pinchasof, O., & Ziv, Y. (2017). Tracking the Same Neurons across Multiple Days in Ca²⁺ Imaging Data. *Cell Reports*, 21(4), 1102–1115. <https://doi.org/10.1016/j.celrep.2017.10.013>

- Simantov, R., Kuhar, M. J., Uhl, G. R., & Snyder, S. H. (1977). Opioid peptide enkephalin: Immunohistochemical mapping in rat central nervous system. *Proceedings of the National Academy of Sciences*, *74*(5), 2167–2171. <https://doi.org/10.1073/pnas.74.5.2167>
- Slotnick, B. M., McMullen, M. F., & Fleischer, S. (1973). Changes in Emotionality Following Destruction of the Septal Area in Albino Mice. *Brain, Behavior and Evolution*, *8*(4), 241–252. <https://doi.org/10.1159/000124357>
- Swanson, L. W., & Cowan, W. M. (1979). The connections of the septal region in the rat. *Journal of Comparative Neurology*, *186*(4), 621–655. <https://doi.org/10.1002/cne.901860408>
- van der Veldt, S., Etter, G., Mosser, C.-A., Manseau, F., & Williams, S. (2021). Conjunctive spatial and self-motion codes are topographically organized in the GABAergic cells of the lateral septum. *PLoS Biology*, *19*(8), e3001383. <https://doi.org/10.1371/journal.pbio.3001383>
- Vance, M. L. (1990). Growth-hormone-releasing hormone. *Clinical Chemistry*, *36*(3), 415–420.
- Wirtshafter, H. S., & Wilson, M. A. (2020). Differences in reward biased spatial representations in the lateral septum and hippocampus. *ELife*, *9*, e55252. <https://doi.org/10.7554/eLife.55252>
- Wong, L. C., Wang, L., D'Amour, J. A., Yumita, T., Chen, G., Yamaguchi, T., Chang, B. C., Bernstein, H., You, X., Feng, J. E., Froemke, R. C., & Lin, D. (2016). Effective Modulation of Male Aggression through Lateral Septum to Medial Hypothalamus Projection. *Current Biology*, *26*(5), 593–604. <https://doi.org/10.1016/j.cub.2015.12.065>
- Yeates, D. C. M., Leavitt, D., Sujanthan, S., Khan, N., Alushaj, D., Lee, A. C. H., & Ito, R. (2022). Parallel ventral hippocampus-lateral septum pathways differentially regulate

approach-avoidance conflict. *Nature Communications*, 13(1), Article 1.

<https://doi.org/10.1038/s41467-022-31082-0>

Zhou, P., Resendez, S. L., Rodriguez-Romaguera, J., Jimenez, J. C., Neufeld, S. Q.,

Giovannucci, A., Friedrich, J., Pnevmatikakis, E. A., Stuber, G. D., Hen, R., Kheirbek,

M. A., Sabatini, B. L., Kass, R. E., & Paninski, L. (2018). Efficient and accurate

extraction of in vivo calcium signals from microendoscopic video data. *ELife*, 7, e28728.

<https://doi.org/10.7554/eLife.28728>